Full length article

Allogenic tissue-specific decellularized scaffolds promote long-term muscle innervation and functional recovery in a surgical diaphragmatic hernia model

Caterina Trevisan [a,b], Edoardo Maghin [a,b], Arben Dedja [c], Paola Caccin [d], Niccolò de Cesare [a,e,f], Chiara Franzin [a], Daniele Boso [a,d], Paola Pesce [g], Federico Caicci [h], Francesco Boldrin [h], Luca Urbani [i,j,k], Paolo De Coppi [k,l], Michela Pozzobon [a,b], Piero Pavan [a,e,f], Martina Piccoli [a,d,*]

[a] Fondazione Istituto di Ricerca Pediatrica Città della Speranza, Corso Stati Uniti 4, 35129 Padova, Italy
[b] Department of Women and Children Health, University of Padova, Via Giustiniani 2, 35127 Padova, Italy
[c] Department of Cardiac Thoracic Vascular Sciences and Public Health, University of Padova, Via Giustiniani 2, 35127 Padova, Italy
[d] Department of Biomedical Sciences, University of Padova, Via Bassi 58/B, 35121 Padova, Italy
[e] Department of Industrial Engineering, University of Padova, Padova, Italy
[f] Centre for Mechanics of Biological Materials, University of Padova, Via Gradenigo, 6/a – 35131 Padova, Italy
[g] Department of Medicine, University of Padova, Via Giustiniani 2, 35127 Padova, Italy
[h] Department of Biology, University of Padova, Via Bassi 58/B, 35121 Padova, Italy
[i] Institute of Hepatology, The Foundation for Liver Research, 111 Coldharbour Lane, SE5 9NT London, United Kingdom
[j] Faculty of Life Sciences & Medicine, King's College, London, United Kingdom
[k] Stem Cells & Regenerative Medicine Section, Developmental Biology & Cancer Programme, UCL Great Ormond Street Institute of Child Health, 30 Guilford St, WC1N 1EH London, United Kingdom
[l] Specialist Neonatal and Paediatric Surgery, Great Ormond Street Institute of Child Health, London, United Kingdom

ARTICLE INFO

ABSTRACT

Congenital diaphragmatic hernia (CDH) is a neonatal defect in which the diaphragm muscle does not develop properly, thereby raising abdominal organs into the thoracic cavity and impeding lung development and function. Large diaphragmatic defects require correction with prosthetic patches to close the malformation. This treatment leads to a consequent generation of unwelcomed mechanical stress in the repaired diaphragm and hernia recurrences, thereby resulting in high morbidity and significant mortality rates. We proposed a specific diaphragm-derived extracellular matrix (ECM) as a scaffold for the treatment of CDH. To address this strategy, we developed a new surgical CDH mouse model to test the ability of our tissue-specific patch to regenerate damaged diaphragms. Implantation of decellularized diaphragmatic ECM-derived patches demonstrated absence of rejection or hernia recurrence, in contrast to the performance of a commercially available synthetic material. Diaphragm-derived ECM was able to promote the generation of new blood vessels, boost long-term muscle regeneration, and recover host diaphragmatic function. In addition, using a GFP + Schwann cell mouse model, we identified re-innervation of implanted patches. These results demonstrated for the first time that implantation of a tissue-specific biologic scaffold is able to promote a regenerating diaphragm muscle and overcome issues commonly related to the standard use of prosthetic materials.

Statement of significance

Large diaphragmatic hernia in paediatric patients require application of artificial patches to close the congenital defect. The use of a muscle-specific decellularized scaffold in substitution of currently used synthetic materials allows new blood vessel growth and nerve regeneration inside the patch, supporting new muscle tissue formation. Furthermore, the presence of a tissue-specific scaffold guaranteed long-term muscle regeneration, improving diaphragm performance to almost complete functional recovery. We believe that diaphragm-derived scaffold will be key player in future pre-clinical studies on large animal models.

* Corresponding author at: Tissue Engineering Lab, Fondazione Istituto di Ricerca Pediatrica Città della Speranza, Corso Stati Uniti 4, 35127 Padova, Italy.
E-mail address: m.piccoli@irpcds.org (M. Piccoli).

1. Introduction

Congenital diaphragmatic hernia (CDH) is a severe neonatal defect with an incidence of 1/2500–3000 births, accounts for approximately 8% of the known major congenital anomalies, and possesses important socioeconomic impact [1–3]. In CDH, defect in diaphragm development leads to herniation of abdominal organs into the thoracic cavity and partial failure in lung development. The consequent lung hypoplasia is the cause of the 50% neonatal mortality and long-term morbidity associated with CDH [4]. Despite the severity of the disease, the genetic and cellular etiology of this birth defect is not yet completely understood [5–7].

Regardless of the origin of CDH, infants with this defect undergo surgery early after birth to repair the defect and position the abdominal organs back in their anatomical site. Numerous reconstructive techniques of closure have been described using prerenal fascia, rib structures, and various thoracic and abdominal wall muscle flaps [8–10]. Other materials including absorbable and nonabsorbable meshes have also been used. Currently, the implantation of prosthetic materials, especially of expanded polytetrafluoroethylene (ePTFE) patches, has become the standard procedure to close up large defects in children with CDH [11]. Unfortunately, these materials face the major issues of lack of growth and integration with the surrounding muscle with an associated high rate of hernia recurrence (up to 40%). Moreover, several long-term problems remain to be solved after this kind of surgery: common reported outcomes are severe gastro-esophageal reflux with a need for fundoplication (9–24%), small bowel obstruction (5–37%), and chest wall deformities (6–67%) [12–14].

In recent years, it has been suggested that transplantation of scaffolds composed of extracellular matrix (ECM) proteins promotes repair of injured skeletal muscle by providing a structural and biochemical mold [15]. For congenital muscle defect treatment, research has documented the use of biological scaffolds composed of a sheet of acellular matrix (i.e., Surgisis®) that can provide the desired support and reduce the occurrence of complications resulting from prosthetic and nonabsorbable implants. In preclinical studies, these scaffolds seemed to be an alternative to ePTFE [16]; however, large clinical studies failed to show improvement in the recurrence rate when acellular matrixes were used [16,17]. If recurrences after ePTFE implantation are due to the imbalance between the growth of the infant and the presence of a permanent material, re-herniation for acellular patches may be related to a too rapid degradation of the construct. A tissue-engineered system capable of restoring near-normal mature muscle, vasculature, and ECM composition in the defective diaphragm has yet to be achieved. Moreover, attaining *de novo* innervation of regenerated myofibers remains a critical step for functional restoration of skeletal muscle injuries or defects. All these matters prompt the need for alternative scaffolds that are more resistant to degradation leastwise defect occlusion and complete tissue regeneration.

In this scenario, we investigated the use of a tissue-specific scaffold using decellularized diaphragm muscle. We previously described how such decellularized ECM (dECM) displays important biological features, from pro-angiogenic properties [18] to the attraction and activation of myogenic progenitor cells upon implantation in noninjured models [19]. In this original work, we describe how the dECM obtained from decellularization of murine diaphragms efficiently supported muscle re-growth and restoration by using a surgical model of large-defect diaphragmatic hernia in mice published for the first time. Long-term analyses demonstrated increased and prolonged local myogenic activity when implanting patches of decellularized diaphragm with regard to patches of currently used prosthetic material, with important repercussion on nerve attraction, muscle maturation, and functional recovery, supporting possible translation in future clinical practice for the treatment of diaphragmatic defects.

2. Material and methods

Additional details relating to materials and methodology are provided in Supplementary information.

2.1. Animals

All surgical procedures and animal husbandry were carried out in accordance with University of Padova's Animal care and Use Committee (protocol number 67/2011 approved on 21 September 2011, and 1103/2016-PR approved on 15 November 2016) and were approved by the Ministry of Health in accordance with the Italian Law on the use of experimental animals (D·Lgs. 26/2014). The animals used as donors were 12-week-old C57BL/6j male and female, while the recipients were 12-week-old BALB/c male and female (n = 78).

2.2. Decellularization

Diaphragm muscles were treated with three cycles of the detergent-enzymatic treatment (DET) as previously described [19]. Briefly: samples were washed 2 times in 1X sterile phosphate-buffered saline (PBS, Gibco-Fisher Scientific) and then placed in deionized water (the first step of the decellularization process). Each DET cycle involved deionized water at 4 °C for 24 h, 4% sodium deoxycholate (Sigma) at room temperature (RT) for 4 h, and 2000 kU DNase-I (Sigma) in 1 M NaCl (Sigma) at RT for 3 h, for a total of 3 consecutive DET cycles.

2.3. Surgical model

BALB/c mice were operated in general anesthesia. After a median superior incision, a 3x5 mm hole was surgically created in the left side of the native diaphragm. Afterwards, the defect was closed using either dECM or ePTFE as control. Organs were then repositioned into the abdominal cavity, the abdominal wall was closed in two layers, and the animals were left to wake up under a heating lamp (see Supplementary Fig. 1). Survived mice were euthanized by cervical dislocation at 2 (n = 8), 5 (n = 7), 15 (n = 8), 30 (n = 8), and 90 (n = 10) days postsurgery. Complete methodology is provided in the supplementary materials.

A transgenic mouse expressing cytosolic eGFP under the S100B protein [20] was used to analyze Schwann cell migration and nerve attraction. These mice were analyzed only after 90 days postsurgery (n = 9).

2.4. Ultrasonography

After 30 and 90 days from surgery, thoracic and abdominal subcostal ultrasonography was performed for all the animals using a high-resolution echo machine with a 30 MHz probe (Vevo® 2100 VisualSonics, Toronto, Canada). Untreated mice were analyzed as control (Ctrl). Animals were chest shaved and anesthetized with 3% isoflurane; temperature-controlled anesthesia was maintained with 1.5% isoflurane. Two-dimensional cine loops and M-mode cine loops of the right and left hemi-diaphragms were recorded. Diaphragm excursion (in mm) was measured from M−mode cine loops of the right and left hemi-diaphragm. A single operator imaged all mice.
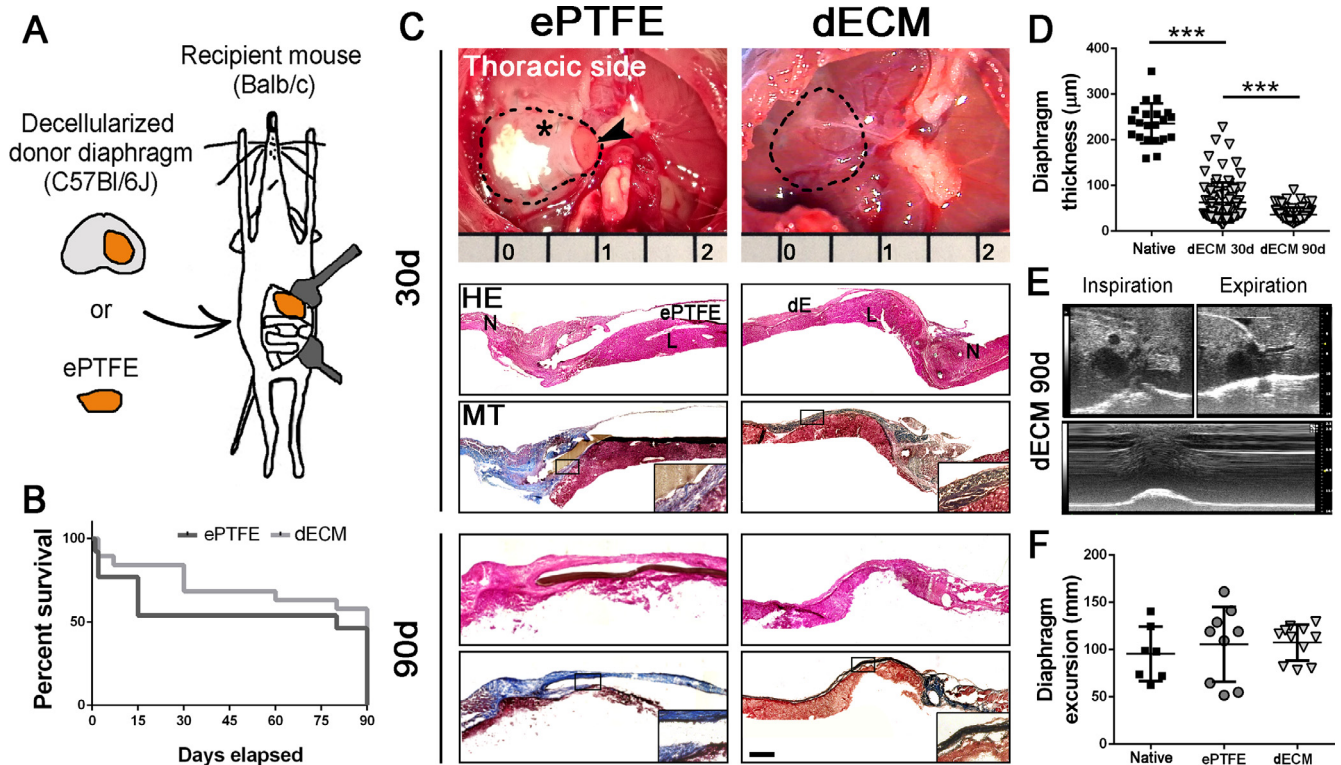
Fig. 1. Gross appearance, morphological, and *in vivo* functional analyses of treated diaphragms. A Schematic representation of collection and transplantation of biologic and synthetic patches. B Surgical CDH survival rate. C Gross appearance (thoracic view) and histology (HE: hematoxylin and eosin; MT: Masson's trichrome) of ePTFE- and dECM-treated diaphragms at 30 and 90 days postsurgery. Dotted line indicates the applied patch. Arrowhead indicates liver herniation. Asterisk indicates fibrotic capsule. D Diaphragm thickness analysis; native is for healthy muscle. E Example of ultrasound echography of dECM-treated diaphragm 90 days after surgery. F Treated diaphragm movement ability measured by ultrasound echography and expressed as percent of excursion with regard to healthy untreated muscles (native). N: native muscle; L: liver; dE: dECM. Scale bar: 100 μm. ***p < .001; ns: not significant.

2.5. In silico analyses of the biomechanical response of repaired diaphragms

We developed different Finite Element Method (FEM)-based numerical models of mice diaphragms (ABAQUS CAE and Dassault Systémes). In particular, we obtained a model of a healthy diaphragm and two models of diaphragms repaired with ePTFE and dECM patch according to a computational approach proposed in a previous work [21]. The model of a healthy diaphragm was defined using anatomical data and echographic images. For healthy and repaired diaphragms, we assumed the same geometry (excluding ePTFE/dECM implant) and the same mechanical properties for muscle tissue and central tendon (Fig. 2A). Suitable constitutive models were adopted to describe active/passive mechanical response of muscle tissue, as well as the passive response of central tendon and ePTFE/dECM patch. The biomechanical response of healthy and repaired diaphragms was analyzed for eupnea condition. Complete methodology is provided in the supplementary materials.

2.6. Histology and immunofluorescence

Histological and immunofluorescence analyses were performed on frozen sections (7–10 μm thick) using primary and secondary antibodies listed in Supplementary Table 1. Complete methodology is provided in the supplementary materials.

2.7. Real-time PCR

Real-time PCR cycles were performed using a LightCycler II (Roche, Monza, Italy). Reactions were carried out in triplicate using Platinum™ SYBR™ Green qPCR SuperMix-UDG (Invitrogen) and 2 μl of primers (Supplementary Table 2), a mix of FW + REV (final concentration, 300/300 nM). Complete methodology is provided in the supplementary materials.

2.8. Mouse phrenic nerve hemi-diaphragm assay and diaphragmatic muscle function analysis

The assay was performed using treated (n = 3 ePTFE; n = 4 dECM) and untreated hemi-diaphragms. The mouse phrenic nerve hemi-diaphragm preparation was set up as previously described [22]; briefly, the diaphragm muscle was dissected with both the phrenic nerves completely functional and then separated as two halves; the central tendon was connected to a transducer; each phrenic nerve was inserted into platinum ring electrodes. In this setup, cotton wire was connected to the phrenic nerve and passed through the two platinum rings of the stimulating electrode. Using a micromanipulator, the electrodes were moved inside the stimulation chamber. Then, the cotton was thread until the phrenic nerve was in contact with the rings. The nerve was completely immersed into the solution and placed ideally perpendicular to the muscle, thus avoiding excessive tension. The electrodes were not in contact with the muscle to prevent direct stimulation of muscle fibers. An additional couple of electrodes was inserted and used to directly stimulate the muscle only at the end of the nerve stimulation experiment to confirm the force values recorded. The stimulation parameters were set up as follows: 5 V, 0.1 ms width, 0.1 Hz for nerve; 30 V, 0.5 ms width, 0.1 Hz for muscle.

To estimate the twitch stress by considering also the size of the specimen, orientation of the fibers, and position and size of the possible implant, we developed FEM models of two pairs of tested
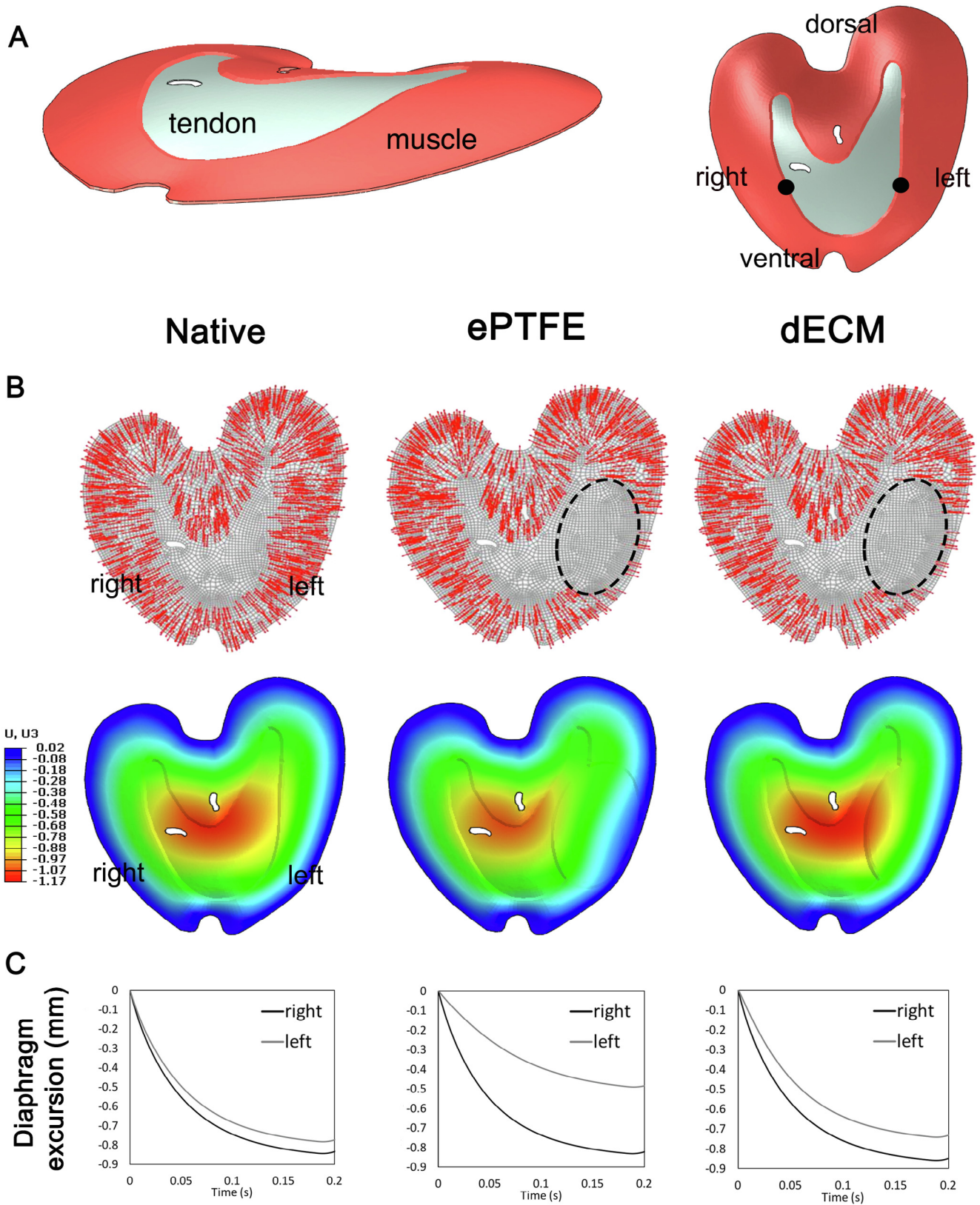
Fig. 2. Modeling of application of ePTFE vs. diaphragm dECM patches. A Finite element model of the mouse diaphragm. Ventral, dorsal, right, and left indicate the anatomical side. B Diaphragm muscle fiber direction (red arrows) and patch highlighted with dotted ellipse (patch is placed in the left hemi-diaphragm); color map of the diaphragm displacement along the caudal–cranial direction (mm) at the maximum contraction of the diaphragm in healthy controls those and repaired with ePTFE and dECM patches; the color bar range is 0.02 mm (blue, minimum displacement) to 1.17 mm (red, maximum displacement). C Diaphragm excursion in the caudal–cranial direction (mm) versus time (s) of right (dark gray line) and left (light gray line) hemi-diaphragms in healthy and ePTFE- and dECM-treated muscles. The excursion of the hemi-diaphragms is described by plotting the displacements of the two points shown in figure A. (For interpretation of the references to color in this figure legend, the reader is referred to the web version of this article.)

samples (treated and untreated hemi-diaphragms) by adopting the same constitutive models described in Section 2.5 and Supplementary materials. Sample morphology and size, as well as boundary conditions, mimicked the setup of the experimental testing. We fitted the numerical response of the models to the experimental data by iteratively changing the value P_0 and the activation function $f_a(t)$ – as under isometric conditions, the force–length function f_l and the force–velocity function f_v are close to unit (see Supplementary materials for the definition of these parameters). In this way, the correct twitch force experimentally measured over time was obtained and the corresponding twitch stress $P_t = P_0 \cdot f_a(t)$ deduced.

2.9. Statistical analysis

All statistical analyses were performed using GraphPad Prism 5 (GraphPad Software). For statistical analysis, unpaired t-tests and one-way ANOVA (followed by Bonferroni post-hoc test) were used. All error bars are presented as s.e.m.; $^*p < 0.05$; $^{**}p < 0.01$; $^{***}p < 0.001$.

3. Results

3.1. Surgical diaphragm hernia mouse model

A new surgical mouse model of large diaphragm hernia was established and developed to test the decellularized scaffold as a new treatment strategy for the repair of defective diaphragms. After intubation, a 3x5 mm defect was surgically created in the left hemi-diaphragm to remove approximately 1/3 of the diaphragm. A hernioplasty was performed with ePTFE or dECM patches stitched to the residual and pericostal native diaphragm (Supplementary Fig. 1). Mice treated with ePTFE were used as control, as this prosthetic material is commonly used in CDH repair. C57BL/6j mice were used as donors of dECM patches, whereas BALB/c mice were chosen as recipients to perform allogeneic transplantation (Fig. 1A). The overall survival rate of the surgery was 64%. In Fig. 1B, the survival rate was calculated at 90 days post-transplantation. A slight, but not significant, improvement in survival rate after biologic patch application was observed, with 57% survival in the dECM-treated group and 46% survival in the ePTFE-treated group.

3.2. Clinical aspects and diaphragm morphological characterization

Twenty percent of the survived ePTFE-treated animals presented herniation of the liver post-transplantation (Fig. 1C), whereas none of the dECM-treated mice showed re-herniation. Macroscopically, no signs of rejection or formation of fibrotic tissue (deposition of collagen fibers) were detected in dECM-treated diaphragms. On the contrary, all the ePTFE-treated animals presented a capsule of fibrotic tissue around the synthetic scaffolds on both thoracic and abdominal sides. Histological analyses confirmed the presence of fibrotic tissue in the control group, with a clear scarring process around ePTFE patches at both 30 and 90 days post implantation (Fig. 1C, left). Evident reabsorption of the scaffold was registered in the dECM-treated group. As expected, dECM patches were gradually remodeled, hence losing approximately 85% of initial thickness 90 days after surgery (Fig. 1D), which confirms a finding previously observed in a scaffold degradation study in vivo without a diaphragm defect [19]. Nevertheless, this important change had no effect on mice diaphragm excursion capacity, which, by ultrasound analysis, proved to be increasingly efficient, with no statistical difference with regard to untreated animals (native) or ePTFE-treated group (Fig. 1E and F). Notably, the

ePTFE-treated group presented a wide range of excursion ability values, with high variability and strong differences among animals.

3.3. In silico analyses of the biomechanical response of repaired diaphragms

Numerical analyses allowed to better evaluate discrepancies among ePTFE-treated animals in terms of diaphragm excursion ability and the difference with the dECM-treated group (Fig. 2A). The estimated excursion of the diaphragms in eupnea breath cycle showed that the ePTFE-treated diaphragm had larger asymmetry than the healthy counterpart (Fig. 2B, bottom). In fact, while the excursion of the two hemi-diaphragms in healthy muscle was similar, the ePTFE-repaired hemi-diaphragm showed a large excursion decrease, which is estimated in approximately 37% of the healthy muscle (Fig. 2C). On the contrary, in dECM-treated muscle, this asymmetry was limited, with a reduction of only approximately 5% in the repaired hemi-diaphragm with regard to healthy diaphragm control (Fig. 2C). This behavior can be attributed to the larger stiffness of ePTFE implant with regard to dECM, although both have no contractile properties. The large stiffness of ePTFE implant is also reflected into a reduced change in volume of the pulmonary cavity. Finally, the last main consequence is the increase of mechanical stress in the muscle tissue surrounding the implant.

3.4. Analyses of immunoreaction and fibrosis response

Given the differences in the gross appearance of ePTFE- and dECM-treated diaphragms and the well-known paradigm of foreign body reaction on application of synthetic materials [23,24], we decided to further investigate the local immune response and fibrogenesis in the treated animals. First, we analyzed cell proliferation in damaged muscles and evaluated the expression of Ki67 marker, which showed similar levels between the two groups, both at early and at late time points (Fig. 3A–D, Supplementary Table 3); this confirms that cell activation was strongly related to the surgical procedure. The same trend was determined when the general innate immune reaction was investigated through molecular analysis of macrophage activation. At early time points, the expression of several markers of activated macrophages (i.e., Nos2, Arg1, Mrc1, Il1B, Tnfa, and Tgfb) was uniformly upregulated in both ePTFE- and dECM-treated diaphragms, thereby highlighting that the surgical procedure stimulated an initial phase of inflammation and a broad immune response (Supplementary Fig. 2). Conversely, 15 days after patch application, the monocyte chemoattractant protein 1 (Mcp1) expression increase was significantly higher in the ePTFE-treated group than in the dECM-treated group (Fig. 3E). The Mcp1 expression gradually decreased in both types of treatment in later time points, reaching the values of untreated samples (CTRL). This phenomenon was faster and more pronounced in dECM-treated diaphragms and slower in ePTFE-treated samples. The overexpression of this soluble factor was associated with the adhesion and engagement of different types of monocytes/-macrophages, with the activation of subsequent events of the foreign body reaction. We considered the difference in Mcp1 expression levels at 15 days as biologically significant, as this difference can be related to the higher amount of macrophages (CD68 + cells) found at both 30 and 90 days in ePTFE-treated samples, thus indicating a more inflammation when the synthetic patch was used (Fig. 3A-D; Supplementary Table 3). The resulting innate immune activation evidenced a strong foreign body reaction against prosthetic nonresorbable patches. The mechanism of reaction was confirmed by H&E and anti-CTGF (connective tissue growth factor) staining, that the results of which indicated the presence of fusing macrophages and giant cells only in the capsule around ePTFE implants (Fig. 3F).

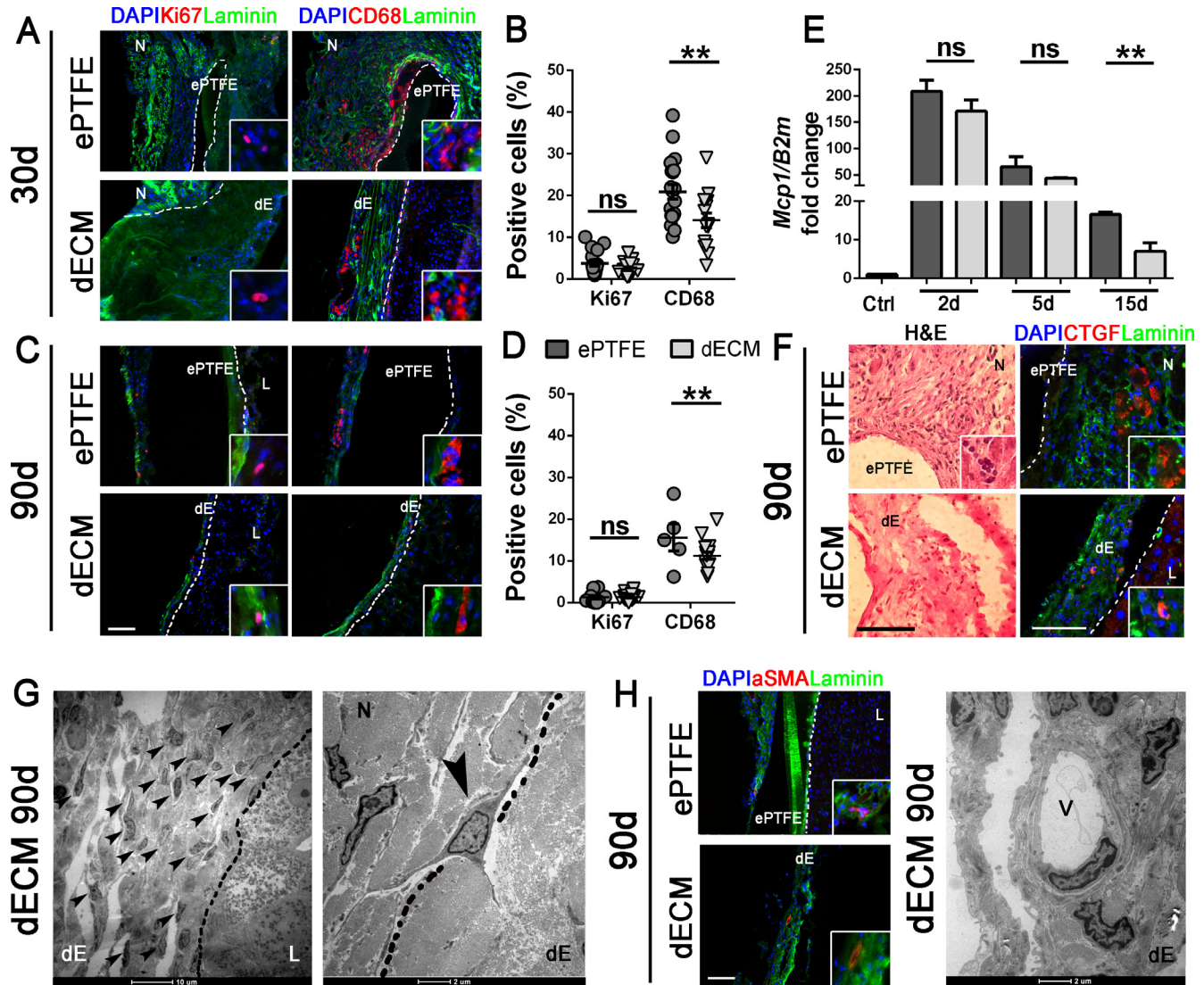**Fig. 3.** Immune response, fibrosis, and vascularization after patch implantation. A-C Immunofluorescence of proliferating (Ki67) cells, macrophages (CD68), and laminin in the treated diaphragms after 30 and 90 days of patch implantation. Nuclei were counterstained with DAPI. B-D Percentage of Ki67 + and CD68 + cells in the treated groups. E *Mcp1* gene expression in treated diaphragms at early time points. F Hematoxylin and eosin stain demonstrated the presence of inflammatory cells in the capsule around ePTFE; giant cells appeared in the enlargement. Immunofluorescence of CTGF + cells. G TEM of implanted dECM 90 days postsurgery: arrowheads indicate migrated cells from native muscle inside dECM. H Immunofluorescence of vessels (aSMA) and laminin in treated diaphragms after 90 days and TEM of a representative vessel inside implanted dECM. Nuclei were counterstained with DAPI. Ctrl: healthy untreated diaphragms. N: native muscle; dE: dECM; L: liver; V: vessel. Where not indicated, scale bar: 100 μm. Statistical analyses: *p < .05; **p < .01; ns: not significant.

3.5. Cell homing and angiogenesis

Formation of an extended vascular network is mandatory to sustain the integration and growth of an implanted engineered tissue [25]. We previously demonstrated that decellularized diaphragm ECM was able to attract different types of cells and induce angiogenesis [18]. In this new model, cell invasion and formation of new capillaries were analyzed 90 days post-surgery by transmission electron microscopy (TEM) and immunofluorescence (Fig. 3G,H). Important changes occurred in the treated diaphragms, and dECM underwent evident modifications; thus, we used TEM to analyze in detail some of these transformations (Supplementary Fig. 3). A remarkable number of cells migrated from the surrounding native muscle into the implanted dECM (Fig. 3G and Supplementary Fig. 3A). It was not possible to precisely quantify the distance covered by the host cells inside the applied patch, but it was evident that different types of cells were present far from

the defect edges, and many of the cells were found in the center of the patch, which suggests a quite complete colonization. Among these cells, αSMA + cells and completely structured vessels were found inside the dECM patches 90 days after transplantation (Fig. 3H and Supplementary Fig. 3B), while no cell homing or angiogenesis was detected in ePTFE patches.

3.6. Myogenic regeneration

As the main desired ability of a tissue-engineered construct should be to stimulate host tissue regeneration, we analyzed the activation of the myogenic pathway at early and late time points. Gene and protein expression was determined by collecting the total hemi-diaphragms containing the patches. At early time points (2, 5, and 15 days), no differences were registered in the upregulation of the analyzed genes *Pax7*, *MyoD*, *Myf5*, and *MyoG* (Supplementary Fig. 4), thus indicating that the muscle self-regenerating
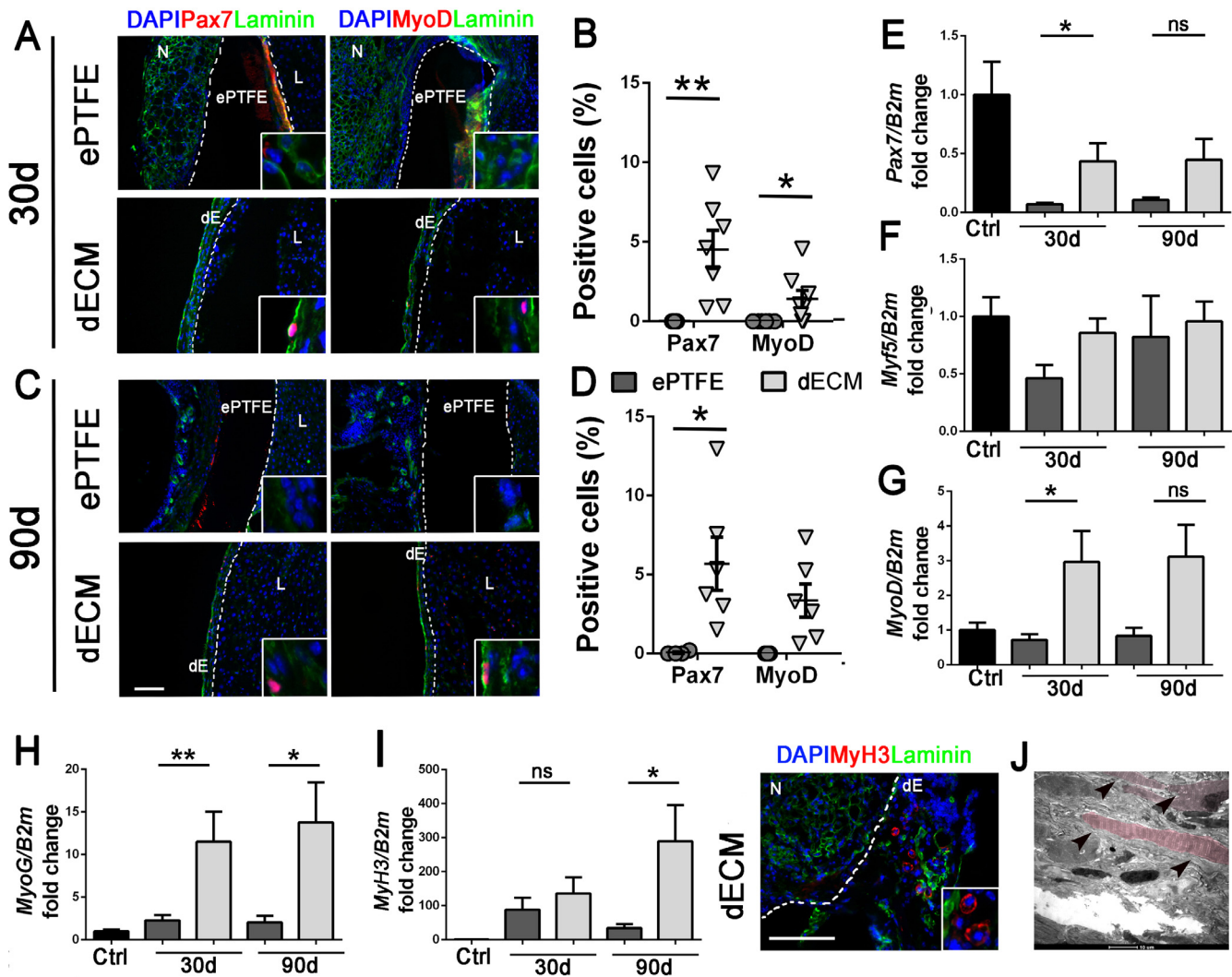
Fig. 4. Decellularized ECM patch long-term myogenic activation. A-D Immunofluorescence and Pax7 and MyoD expression in ePTFE- and dECM-treated diaphragms at 30 and 90 days postimplantation. E-G Molecular analyses of early myogenic gene expression (*Pax7, Myf5, and MyoD*) in treated diaphragms. H-I Molecular analysis and immunofluorescence against late myogenic cell markers (*MyoG* and *MyH3*) and myotubes (MyH3). J Transmission electron microscopy analysis of myofibers (arrowheads) inside the implanted dECM. Ctrl: healthy untreated diaphragms. N: native muscle; dE: dECM; L: liver. Where not indicated, scale bar: 100 μm. Statistical analyses: *p < .05; **p < .01; ns: not significant.

ability post-injury was independent of the patch used. At late time points (30 and 90 days post-transplantation), dECM-treated diaphragms presented an upregulation of early and late myogenic markers compared to ePTFE (Fig. 4A–D). Pax7- and MyoD-positive cells were detected inside dECM (Supplementary Table 3), while the tissue surrounding containing ePTFE patch resulted always negative for these two myogenic progenitor markers. This was confirmed by molecular analyses, where *Pax7, Myf5,* and *MyoD* transcripts were overexpressed in dECM-treated diaphragms with regard to ePTFE (Fig. 4E–G). The fluctuations in the expression of *Pax7* and *MyoD* are related to dECM samples because after 90 days, the expression of stem cell genes and transcription factors also slowly decreases in this type of treatment. This is a predictable behavior, as these markers need to reach a balance after a strong and sustained activation because this also occurs physiologically after muscle regeneration. Importantly, markers responsible for skeletal muscle fiber maturation, namely, *MyoG* and *MyH3*, were also significantly upregulated in dECM-treated diaphragms (Fig. 4H and I) in associated with initial fusion of myogenic progenitor cells (Supplementary Fig. 3C) and new muscle fiber formation inside the dECM scaffold (Fig. 4I and J).

3.7. Diaphragm muscle functionality

We then investigated if the local myogenic activation was linked to the restoration of diaphragm muscle function. Muscle twitch was analyzed 90 days after ePTFE and dECM patch implantation in a well-established *ex vivo* model, the phrenic nerve hemi-diaphragm assay (Fig. 5A). In this assay, despite the phrenic nerves being transected and disconnected from the animal's nervous system, their ability to conduct an electrical stimulus was still present. Indeed, the applied electrodes were conceived to allow a supra-maximal electrical stimulus that was able to depolarize the phrenic nerve. From the contact point, the nerve was able to propagate the depolarization phenomenon and to stimulate the neuromuscular junction, thereby causing neurotransmitter release and the consequent muscle contraction. The ratio between twitch amplitude developed by treated and untreated hemi-diaphragms from the same mouse was taken as a measure of force recovery. The numerical simulation of some experimental tests made it possible to normalize the response of hemi-diaphragms, considering muscle sample morphology, geometry, and fiber orientation, as well as shape and size of the applied patch (Fig. 5B and C). In this way,
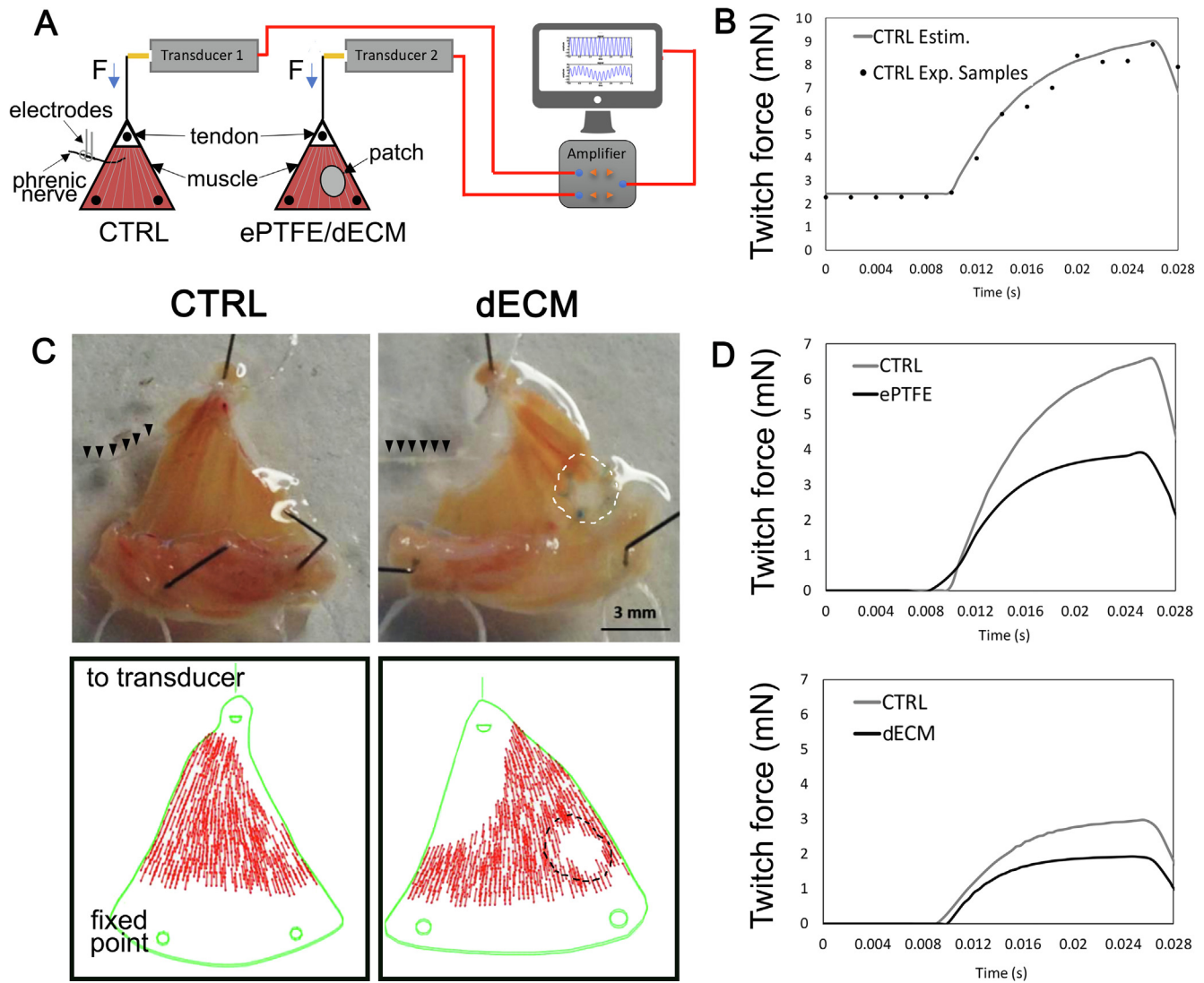
Fig. 5. Diaphragm functionality after patch implantation. A Schematic representation of the experimental mouse phrenic nerve hemi-diaphragm assay system. Electrodes for phrenic nerve stimulation are used for both control (CTRL) and treated (ePTFE/dECM) diaphragms. B Validation of the FEM model through the comparison of CTRL twitch force estimation (CTRL Estim.) and twitch force experimental data (CTRL Exp. Samples). C Images of a single control hemi-diaphragm (CTRL) and hemi-diaphragm repaired with biological patch (dECM); black arrowheads indicates the phrenic nerve. FEM models of the two muscle portions, CTRL and dECM, respectively; red arrows show the local spatial orientation of muscle fibers (not the density). D Twitch force F (mN) acquired with a force transducer versus time (s) produced by the diaphragm portions, repaired with ePTFE patch and with dECM patch, respectively. The latter two diaphragms are plotted by subtracting the basal force from the total twitch force. The comparison of the twitch force should be made between treated hemi-diaphragm and contralateral of the same animal. However, the twitch force is affected by contractile properties of muscle fiber geometry and size of the hemi-diaphragms. A normalization of the twitch force can be obtained using FEM models, as reported in Sections 2.8 and 3.7, to deduce the twitch stress. (For interpretation of the references to color in this figure legend, the reader is referred to the web version of this article.)

we estimated more physiological force production in dECM-treated diaphragms, with twitch stress P_t closer to the untreated tissue ($P_t^{ECM} = 0.53P_t^{ctrl}$), and lower muscle contraction ability was estimated in ePTFE-treated diaphragms, with an overall reduction of approximately 65% ($P_t^{ePTFE} = 0.35P_t^{ctrl}$; Fig. 5D). This suggested that decellularized ECM patches were more efficient in sustaining host tissue regeneration and function recovery, even if the limited number of cases analyzed and the variance of data did not allow to find statistically significant difference.

3.8. Nerve attraction and re-growth

Presence of neuromuscular junctions and innervations is an essential feature of active and functional skeletal muscle tissue [26,27]. To test whether the force generation in restored diaphragm muscles was associated with re-innervation, we investigated the presence of neuronal marker inside dECM. Schwann cells are well-known precursors of nerve regeneration [28]; with the advantage of a mouse model carrying the GFP under the control of S100 protein, a specific Schwann cell marker, infiltration of green cells was identified 90 days post-surgery from the surrounding native muscle to the implanted patch (Fig. 6A). To deeply understand the relationship between Schwann cells and the surrounding tissue, we performed a CLEM (correlative light and electron microscopy) analysis [29]: using the protocol described in Supplementary Fig. 5, we selected a group of Schwann cells clearly located inside the dECM and visualized the same cells at high magnification by TEM (Fig. 6B). This analysis underlined that Schwann cells were infiltrated inside the implanted patch together with myogenic cells and other cell types, hence indicating again a situation of active and complete tissue regeneration (Supplementary Fig. 6)
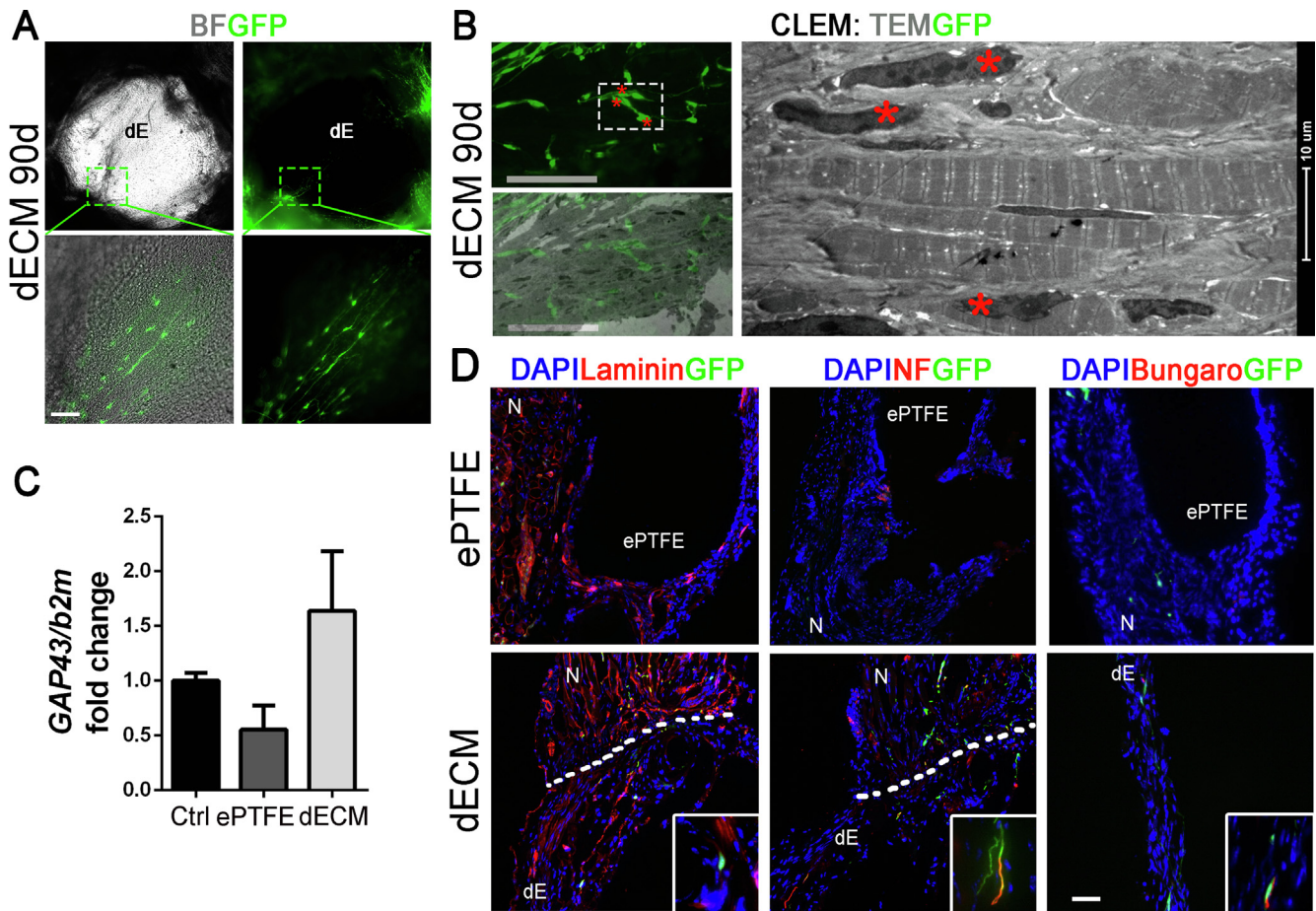
Fig. 6. Decellularized ECM nerve attraction and re-growth at 90 days post-surgery. A Picture of bright field (BF) and GFP expression of dECM-treated diaphragm at 90 days post-surgery. Lower panels: enlargement of dashed box, showing Schwann cells inside the implanted patch. B Correlative light and electron microscopy (CLEM) analysis; fluorescence imaging of a group of Schwann cells migrated in the dECM (left, up); superposition of low-magnification TEM and fluorescence image, scaled to the same proportions (left, bottom); high magnification (1850x) of the same cells (right). Red stars indicate Schwann cells. C Molecular analysis of *GAP43* expression in treated samples. D Immunofluorescence of ePTFE- and dECM-treated diaphragms; GFP expression indicates the presence of migrated Schwann cells. NF: neurofilament; Bungaro: α– Bungarotoxin. N: native muscle; dE: dECM; S: Schwann cell. Scale bar: 100 µm. Statistical analyses: * p < .05; ** p < .01; ns: not significant. (For interpretation of the references to color in this figure legend, the reader is referred to the web version of this article.)

As Schwann cell migration is conditioned by tissue ECM characteristics and properties, we verified *in vitro* the ability of Schwann cells to recognize and migrate inside our dECM, a mechanism that is inhibited when the synthetic patch is used (Supplementary Fig. 7). Further *in vivo* analyses demonstrated that there was an increased expression of growth-associated protein 43 (*GAP43*), a specific marker of axonal regeneration, in dECM-treated muscles compared to ePTFE-treated ones (Fig. 6C). Moreover, immunofluorescence analysis demonstrated the co-expression of neurofilament and GFP inside the implanted dECM patch (Fig. 6D), suggesting initial re-innervation from the surrounding tissue toward the dECM. Importantly, clusters of acetylcholine receptors were also detected by α– bungarotoxin, which indicates that new neuromuscular junctions could be restored inside the implanted dECM.

4. Discussion

Large diaphragmatic hernia in pediatric patients requires the application of artificial patches to close the congenital defect. The resulting neo-diaphragm is not elastic and therefore nonfunctional, and plastic prosthesis does not grow with the child. This situation leads to hernia recurrences and the need for multiple interventions. Given the current suboptimal methods, we paid attention on the use of decellularized scaffolds specifically obtained from

the diaphragm muscle. The importance of using tissue-specific naturally derived scaffolds to obtain a more precise and committed regeneration is reported in literature [30,31]. Moreover, several non-tissue-specific acellular matrices were used to repair CDH (i.e., Permacol™, Surgisis®, and SIS), and despite their biocompatibility and efficiency when used in other tissues, the overall results in terms of drawbacks, and hernia recurrences were not better than those of standard PTFE treatment [16,17,32]. In this study, we showed for the first time the superiority of decellularized diaphragm ECM for the closure of a diaphragmatic defect in a new surgical model of diaphragm hernia, which does not exist in literature. We aimed to investigate the efficacy of this bioscaffold in supporting skeletal muscle regeneration with regard to currently used prosthetic materials, with the prospective of future translation into clinical practice for the repair of diaphragm defects. We previously described the desirable structural, biological, and biomechanical properties of decellularized diaphragm ECM [19]. In this research, we ultimately demonstrated its ability to foster re-innervation and muscle function recovery.

The first important result obtained upon transplantation of dECM-derived patches to repair diaphragm defects was the improvement of clinical outcome with no hernia recurrence detected, while approximately 20% of ePTFE-treated mice presented liver herniation. In addition, despite the use of an allograft dECM, we did not find any sign of rejection after transplantation.

We previously reported that immune-modulation exerted by diaphragm-derived ECM is exerted *through* CD4 + Foxp3 + cell activation [19]. Another study demonstrated that tissue-derived biomaterial scaffolds enhance the development of a pro-regenerative immune environment with implication of adaptive immune cells, specifically mTORC2-dependent CD4 + TH2 T cells, with inhibition of CD68 + macrophage upregulation [33], data confirmed in our diaphragmatic hernia model. On the other side, synthetic patches induced a predictable foreign body reaction, with consequent fibrosis/fibrous capsule development that was completely absent when dECM patches were used. The foreign body reaction is classically characterized by activation of innate immune response prompted by adhesion of proteins and other biomolecules to the surface of the implant, followed by attraction and fusion of macrophages around the foreign body to form giant cells [34,35]. This phenotype is accompanied by overexpression of CTGF and sustained macrophages activation, characteristics that we found to be significantly upregulated in mice treated with ePTFE with regard to those with dECM.

Angiogenesis is a mechanism strictly related to the resolution of the balance between inflammation and muscle regeneration. Numerous studies have shown that the close interaction among endothelial, immune and fibro-adipogenic cells, and myogenic precursors is crucial for good skeletal muscle regeneration [36–38]. We previously reported that decellularized diaphragm ECM possesses several cytokines that confer the biologic scaffold the ability to attract vessels and capillaries *in vivo* [18]. We confirmed the angiogenic properties of decellularized diaphragm ECM also in our model of diaphragm hernia, with α–SMA+ cells and vessels found only inside implanted dECM and not in ePTFE implants, where just little capillaries were noticed in the surrounding fibrotic capsule. This definitely demonstrated that diaphragm-derived scaffolds could be efficiently re-vascularized once implanted *in vivo*.

Activation of efficient local muscle regeneration is a critical outcome of our tissue engineering approach for a complete functional correction of the diaphragm defect. In our mouse model, the surgical injury initially activated a self-regeneration mechanism, which then persisted long term only in dECM-treated animals. In fact, diametrically opposite results were obtained in terms of myogenic pathway activation between ePTFE and dECM implants. Tissue-specific dECM scaffolds were able to induce the entire myogenic program, from activation of Pax7+ stem cells to the formation of myofibers, indicated by the expression of MyH3, a specific marker of newly generated fibers. This process was completely absent in ePTFE-treated diaphragms. This result is of paramount importance, as the regeneration evoked by tissue-specific dECM recapitulates the physiological pathway and, most importantly, persists for a long period, re-enforcing new tissue formation. This strong activation of muscle regeneration translated into an overall amelioration of diaphragmatic function. Using the *ex vivo* model of phrenic nerve hemi-diaphragm assay, we highlighted the specific contractile capacities of the diaphragmatic muscle after surgery. In this system, only dECM-treated diaphragms presented a good twitch force recovery after damage, and importantly, the experimental result was robustly supported by numerical analysis, hence aiming at normalizing treated hemi-diaphragms to the corresponding untreated counterpart to reduce physiological interindividual variation.

It is known from the literature that restoration of muscle function is strongly related to efficient re-innervation of the transplanted construct [39–41]. Re-innervation of muscle fibers in the injured tissue and in transplanted muscle explants can take long time to occur [42], and exercise has been proposed to improve and accelerate muscle function following skeletal muscle injuries [27,30]. On the basis of these suggestions, we hypothesized that a regime of indispensable exercise, as it occurs in the diaphragm muscle, could naturally enhance and stimulate nerve attraction.

Indeed, we found GFP+ Schwann cells migrating from the surrounding muscle tissue to implanted dECM patches. In the peripheral nervous system, Schwann cells produce the myelin sheath, and myelinated Schwann cells can dedifferentiate and drive the regeneration of peripheral axons upon nerve injury [28,43]. This regeneration is strongly related to biologic and biomechanical properties of the ECM surrounding the injured nerve [44,45]. We observed that in our model, Schwann cells easily recognized the implanted biologic patch, thereby promoting their migration inside the scaffold and initial nerve regeneration. This phenomenon is also influenced by the ability of myogenic cells to migrate and form new muscle fibers inside the patch, as it is reported in the literature that muscle fibers can sense whether or not they are innervated and respond to denervation by enhancing their susceptibility to re-innervation [46,47]. At the same time, formation of neuromuscular junctions inside the implanted scaffold, as indicated by the presence of neurofilament and α–bungarotoxin staining, ensured and fostered a continuous maturation of the skeletal muscle compartment [48], establishing a long-lasting positive loop between muscle and the nervous system.

Despite the positive clinical outcome and general functional recovery at 90 days post-transplantation, dECM patches did not activate complete defect regeneration. This was probably due to a persistent imbalance between dECM remodeling and skeletal muscle regeneration, a limit that could be overcome with different kinds of dECM functionalization [49], from loading of selected growth factors for massive recruitment of muscle (stem) cells to the *in vitro* cell engineering of the biologic scaffolds with appropriate progenitors before *in vivo* implantation [30].

5. Conclusion

In conclusion, we believe that these results lay a solid pillar for the tissue engineering approaches for the treatment of CDH, thereby identifying tissue-specific diaphragm-derived ECM as key player in future preclinical studies on large animal models.

Acknowledgments

Appendix A. Supplementary data

Supplementary data to this article can be found online at https://doi.org/10.1016/j.actbio.2019.03.007.

References

[1] M.V. Raval, X. Wang, M. Reynolds, A.C. Fischer, Costs of congenital diaphragmatic hernia repair in the United States-extracorporeal membrane oxygenation foots the bill, J. Pediatr. Surg. 46 (2011) 617–624.
[2] C.P. Torfs, C.J. Curry, T.F. Bateson, L.H. Honore, A population-based study of congenital diaphragmatic hernia, Teratology 46 (1992) 555–565.
[3] M.R. McGivern, K.E. Best, J. Rankin, D. Wellesley, R. Greenlees, M.C. Addor, L. Arriola, H. de Walle, I. Barisic, J. Beres, F. Bianchi, E. Calzolari, B. Doray, E.S.

Draper, E. Garne, M. Gatt, M. Haeusler, B. Khoshnood, K. Klungsoyr, A. Latos-Bielenska, M. O'Mahony, P. Braz, B. McDonnell, C. Mullaney, V. Nelen, A. Queisser-Luft, H. Randrianaivo, A. Rissmann, C. Rounding, A. Sipek, R. Thompson, D. Tucker, W. Wertelecki, C. Martos, Epidemiology of congenital diaphragmatic hernia in Europe: a register-based study, Arch. Dis. Child. Fetal Neonatal Ed. 100 (2015) F137–F144.

[4] B.R. Pober, Overview of epidemiology, genetics, birth defects, and chromosome abnormalities associated with CDH, Am. J. Med. Genet. Part C, Semin. Med. Genet. 145C (2007) 158–171.

[5] V.K. Jordan, T.F. Beck, A. Hernandez-Garcia, P.N. Kundert, B.J. Kim, S.N. Jhangiani, T. Gambin, M. Starkovich, J. Punetha, I.S. Paine, J.E. Posey, A.H. Li, D. Muzny, C.W. Hsu, A.J. Lashua, X. Sun, C.J. Fernandes, M.E. Dickinson, K.P. Lally, R.A. Gibbs, E. Boerwinkle, J.R. Lupski, D.A. Scott, The role of FREM2 and FRAS1 in the development of congenital diaphragmatic hernia, Hum. Mol. Genet. (2018).

[6] A.J. Merrell, B.J. Ellis, Z.D. Fox, J.A. Lawson, J.A. Weiss, G. Kardon, Muscle connective tissue controls development of the diaphragm and is a source of congenital diaphragmatic hernias, Nat. Genet. 47 (2015) 496–504.

[7] Q. Zhu, F.A. High, C. Zhang, E. Cerveira, M.K. Russell, M. Longoni, M.P. Joy, M. Ryan, A. Mil-Homens, L. Bellfy, C.M. Coletti, P. Bhayani, R. Hila, J.M. Wilson, P.K. Donahoe, C. Lee, Systematic analysis of copy number variation associated with congenital diaphragmatic hernia, Proceed. Natl. Acad. Sci. U.S.A. (2018).

[8] R. Horta, T. Henriques-Coelho, J. Costa, J. Estevao-Costa, D. Monteiro, M. Dias, J. Braga, A. Silva, I. Azevedo, J.M. Amarante, Fascicular phrenic nerve neurotization for restoring physiological motion in a congenital diaphragmatic hernia reconstruction with a reverse innervated latissimus dorsi muscle flap, Ann. Plast. Surg. 75 (2015) 193–196.

[9] J.S. Simpson, J.D. Gossage, Use of abdominal wall muscle flap in repair of large congenital diaphragmatic hernia, J. Pediatr. Surg. 6 (1971) 42–44.

[10] R.M. Sydorak, W. Hoffman, H. Lee, C.D. Yingling, M. Longaker, J. Chang, B. Smith, M.R. Harrison, C.T. Albanese, Reversed latissimus dorsi muscle flap for repair of recurrent congenital diaphragmatic hernia, J. Pediat. Surg. 38 (2003) 296–300. discussion 296–300.

[11] L.M. de Kort, K.M. Bax, Prosthetic patches used to close congenital diaphragmatic defects behave well: a long-term follow-up study, Eur. J. Pediat. Surg. Off. J. Aust. Assoc. Pediat. Surg. [et al] = Z. Kinderchir. 6 (1996) 136–138.

[12] S. Janssen, K. Heiwegen, I.A. van Rooij, H. Scharbatke, J. Roukema, I. de Blaauw, S.M. Botden, Factors related to long-term surgical morbidity in congenital diaphragmatic hernia survivors, J. Pediatr. Surg. 53 (2018) 508–512.

[13] C.A. Laituri, C.L. Garey, P.A. Valusek, F.B. Fike, A.J. Kaye, D.J. Ostlie, C.L. Snyder, St Peter SD. Outcome of congenital diaphragmatic hernia repair depending on patch type, Eur. J. Pediat. Surg. Off. J. Aust. Assoc. Pediat. Surg. [et al] = Z. Kinderchir. 20 (2010) 363–365.

[14] K. Yokota, H. Uchida, K. Kaneko, Y. Ono, N. Murase, S. Makita, M. Hayakawa, Surgical complications, especially gastroesophageal reflux disease, intestinal adhesion obstruction, and diaphragmatic hernia recurrence, are major sequelae in survivors of congenital diaphragmatic hernia, Pediatr. Surg. Int. 30 (2014) 895–899.

[15] B.M. Sicari, J.P. Rubin, C.L. Dearth, M.T. Wolf, F. Ambrosio, M. Boninger, N.J. Turner, D.J. Weber, T.W. Simpson, A. Wyse, E.H. Brown, J.L. Dziki, L.E. Fisher, S. Brown, S.F. Badylak, An acellular biologic scaffold promotes skeletal muscle formation in mice and humans with volumetric muscle loss, Sci. Transl. Med. 6 (2014) 234ra58.

[16] E.J. Grethel, R.A. Cortes, A.J. Wagner, M.S. Clifton, H. Lee, D.L. Farmer, M.R. Harrison, R.L. Keller, K.K. Nobuhara, Prosthetic patches for congenital diaphragmatic hernia repair: surgisis vs Gore-Tex, J. Pediat. Surg. 41 (2006) 29–33. discussion 29–33.

[17] R.L. Romao, A. Nasr, P.P. Chiu, J.C. Langer, What is the best prosthetic material for patch repair of congenital diaphragmatic hernia? Comparison and meta-analysis of porcine small intestinal submucosa and polytetrafluoroethylene, J. Pediatr. Surg. 47 (2012) 1496–1500.

[18] M.E. Alvarez Fallas, M. Piccoli, C. Franzin, A. Sgro, A. Dedja, L. Urbani, E. Bertin, C. Trevisan, P. Gamba, A.J. Burns, P. De Coppi, Pozzobon M. Decellularized, Diaphragmatic muscle drives a constructive angiogenic response in Vivo, Int. J. Mol. Sci. 19 (2018).

[19] M. Piccoli, L. Urbani, M.E. Alvarez-Fallas, C. Franzin, A. Dedja, E. Bertin, G. Zuccolotto, A. Rosato, P. Pavan, N. Elvassore, P. De Coppi, M. Pozzobon, Improvement of diaphragmatic performance through orthotopic application of decellularized extracellular matrix patch, Biomaterials 74 (2016) 245–255.

[20] Y. Zuo, J.L. Lubischer, H. Kang, L. Tian, M. Mikesh, A. Marks, V.L. Scofield, S. Maika, C. Newman, P. Krieg, W.J. Thompson, Fluorescent proteins expressed in mouse transgenic lines mark subsets of glia, neurons, macrophages, and dendritic cells for vital examination, J. Neurosci. Off. J. Soc. Neurosci. 24 (2004) 10999–11009.

[21] N. de Cesare, C. Trevisan, E. Maghin, M. Piccoli, P.G. Pavan, A finite element analysis of diaphragmatic hernia repair on an animal model, J. Mech. Behav. Biomed. Mater. 86 (2018) 33–42.

[22] G.N.S. Zanetti, M. Pirazzini, P. Caccin, Mouse phrenic nerve hemidiaphragm assay (MPN), Bio-protocol 8 (2018) 1–12.

[23] E.E. Friedrich, S.T. Lanier, S. Niknam-Bienia, G.A. Arenas, D. Rajendran, J.A. Wertheim, R.D. Galiano, Residual sodium dodecyl sulfate in decellularized muscle matrices leads to fibroblast activation in vitro and foreign body response in vivo, J. Tissue Eng. Regener. Med. (2017).

[24] Ward W. Kenneth, A review of the foreign-body response to subcutaneously-implanted devices: the role of macrophages and cytokines in biofouling and fibrosis, J. Diabetes Sci. Technol. 2 (2008) 768–777.

[25] S. Levenberg, J. Rouwkema, M. Macdonald, E.S. Garfein, D.S. Kohane, D.C. Darland, R. Marini, C.A. van Blitterswijk, R.C. Mulligan, P.A. D'Amore, R. Langer, Engineering vascularized skeletal muscle tissue, Nat. Biotechnol. 23 (2005) 879–884.

[26] A. Aurora, K. Garg, B.T. Corona, T.J. Walters, Physical rehabilitation improves muscle function following volumetric muscle loss injury, BMC Sports Sci., Med. Rehabil. 6 (2014) 41.

[27] N.E. Gentile, K.M. Stearns, E.H. Brown, J.P. Rubin, M.L. Boninger, C.L. Dearth, F. Ambrosio, S.F. Badylak, Targeted rehabilitation after extracellular matrix scaffold transplantation for the treatment of volumetric muscle loss, Am. J. Phys. Med. Rehabil. 93 (2014) S79–S87.

[28] K.R. Jessen, R. Mirsky, The repair Schwann cell and its function in regenerating nerves, J. Physiol. 594 (2016) 3521–3531.

[29] E.V. Polishchuk, R.S. Polishchuk, A. Luini, Correlative light-electron microscopy as a tool to study in vivo dynamics and ultrastructure of intracellular structures, Methods Mol. Biol. 931 (2013) 413–422.

[30] M. Quarta, M. Cromie, R. Chacon, J. Blonigan, V. Garcia, I. Akimenko, M. Hamer, P. Paine, M. Stok, J.B. Shrager, T.A. Rando, Bioengineered constructs combined with exercise enhance stem cell-mediated treatment of volumetric muscle loss, Nat. Commun. 8 (2017) 15613.

[31] S. Shojaie, L. Ermini, C. Ackerley, J. Wang, S. Chin, B. Yeganeh, M. Bilodeau, M. Sambi, I. Rogers, J. Rossant, C.E. Bear, M. Post, Acellular lung scaffolds direct differentiation of endoderm to functional airway epithelial cells: requirement of matrix-bound HS proteoglycans, Stem Cell Rep. 4 (2015) 419–430.

[32] B. Bekdash, B. Singh, K. Lakhoo, Recurrent late complications following congenital diaphragmatic hernia repair with prosthetic patches: a case series, J. Med. Case Rep. 3 (2009) 7237.

[33] K. Sadtler, K. Estrellas, B.W. Allen, M.T. Wolf, H. Fan, A.J. Tam, C.H. Patel, B.S. Luber, H. Wang, K.R. Wagner, J.D. Powell, F. Housseau, D.M. Pardoll, J.H. Elisseeff, Developing a pro-regenerative biomaterial scaffold microenvironment requires T helper 2 cells, Science 352 (2016) 366–370.

[34] J. Cohen, Assay of foreign-body reaction, The J. Bone Joint Surg. Am. 41-A (1959) 152–166.

[35] F.C. Usher, S.A. Wallace, Tissue reaction to plastics; a comparison of nylon, orlon, dacron, teflon, and marlex, AMA Arch. Surg. 76 (1958) 997–999.

[36] L. Arnold, A. Henry, F. Poron, Y. Baba-Amer, N. van Rooijen, A. Plonquet, R.K. Gherardi, B. Chazaud, Inflammatory monocytes recruited after skeletal muscle injury switch into antiinflammatory macrophages to support myogenesis, J. Exp. Med. 204 (2007) 1057–1069.

[37] M. Saclier, S. Cuvellier, M. Magnan, R. Mounier, B. Chazaud, Monocyte/macrophage interactions with myogenic precursor cells during skeletal muscle regeneration, The FEBS J. 280 (2013) 4118–4130.

[38] A. Uezumi, S. Fukada, N. Yamamoto, S. Takeda, K. Tsuchida, Mesenchymal progenitors distinct from satellite cells contribute to ectopic fat cell formation in skeletal muscle, Nat. Cell Biol. 12 (2010) 143–152.

[39] V. Agrawal, B.N. Brown, A.J. Beattie, T.W. Gilbert, S.F. Badylak, Evidence of innervation following extracellular matrix scaffold-mediated remodelling of muscular tissues, J. Tissue Eng. Regener. Med. 3 (2009) 590–600.

[40] I.K. Ko, B.K. Lee, S.J. Lee, K.E. Andersson, A. Atala, J.J. Yoo, The effect of in vitro formation of acetylcholine receptor (AChR) clusters in engineered muscle fibers on subsequent innervation of constructs in vivo, Biomaterials 34 (2013) 3246–3255.

[41] S. Mosole, U. Carraro, H. Kern, S. Loefler, H. Fruhmann, M. Vogelauer, S. Burggraf, W. Mayr, M. Krenn, T. Paternostro-Sluga, D. Hamar, J. Cvecka, M. Sedliak, V. Tirpakova, N. Sarabon, A. Musaro, M. Sandri, F. Protasi, A. Nori, A. Pond, S. Zampieri, Long-term high-level exercise promotes muscle reinnervation with age, J. Neuropathol. Exp. Neurol. 73 (2014) 284–294.

[42] C.H. Lin, Y.T. Lin, J.T. Yeh, C.T. Chen, Free functioning muscle transfer for lower extremity posttraumatic composite structure and functional defect, Plast. Reconstr. Surg. 119 (2007) 2118–2126.

[43] A. Boerboom, V. Dion, A. Chariot, R. Franzen, Molecular mechanisms involved in Schwann cell plasticity, Front. Mol. Neurosci. 10 (2017) 38.

[44] S. Belin, K.L. Zuloaga, Y. Poitelon, Influence of mechanical stimuli on schwann cell biology, Front. Cell. Neurosci. 11 (2017) 347.

[45] M.B. Bunge, A.K. Williams, P.M. Wood, J. Uitto, J.J. Jeffrey, Comparison of nerve cell and nerve cell plus Schwann cell cultures, with particular emphasis on basal lamina and collagen formation, J. Cell Biol. 84 (1980) 184–202.

[46] M.A. Fox, J.R. Sanes, D.B. Borza, V.P. Eswarakumar, R. Fassler, B.G. Hudson, S.W. John, Y. Ninomiya, V. Pedchenko, S.L. Pfaff, M.N. Rheault, Y. Sado, Y. Segal, M.J. Werle, H. Umemori, Distinct target-derived signals organize formation, maturation, and maintenance of motor nerve terminals, Cell 129 (2007) 179–193.

[47] A.H. Williams, G. Valdez, V. Moresi, X. Qi, J. McAnally, J.L. Elliott, R. Bassel-Duby, J.R. Sanes, E.N. Olson, MicroRNA-206 delays ALS progression and promotes regeneration of neuromuscular synapses in mice, Science 326 (2009) 1549–1554.

[48] W. Liu, L. Wei-LaPierre, A. Klose, R.T. Dirksen, J.V. Chakkalakal, Inducible depletion of adult skeletal muscle stem cells impairs the regeneration of neuromuscular junctions, eLife 4 (2015).

[49] S. Mayer, H. Decaluwe, M. Ruol, S. Manodoro, M. Kramer, H. Till, J. Deprest, Diaphragm repair with a novel cross-linked collagen biomaterial in a growing rabbit model, PLoS ONE 10 (2015). e0132021.